Journal of Materials Chemistry A

ROYAL SOCIETY OF CHEMISTRY

PERSPECTIVE

View Article Online
View Journal | View Issue

Cite this: J. Mater. Chem. A, 2023, 11, 20459

Metal–organic frameworks for hydrocarbon separation: design, progress, and challenges

Xiao-Jing Xie, Heng Zeng, Weigang Lu * and Dan Li *

High-purity hydrocarbons are of great importance in various fields, including the electronics and chemical industries; however, the separation of hydrocarbons can be difficult because of their structural and chemical similarities. The established industrial practices of separating hydrocarbons usually involve energy-intensive procedures such as low-temperature distillation. Adsorptive separation using porous materials is deemed a promising alternative technology due to its potential to significantly reduce energy consumption. Porous materials, MOFs in particular, offer versatility in terms of their synthesis and structural design that can be facilely customized to meet the requirements of specific applications. By tailoring pore dimensions, surface functionality, and framework flexibility, MOF materials exhibit high selectivity for specific molecules in the separation and purification of hydrocarbons. With the rapid advances in reticular chemistry and crystal engineering, researchers have gained deep insight into the directional stitching of diverse building blocks, paving the way for the design of tailor-made MOF materials. This perspective summarizes three main strategies for developing MOFs for hydrocarbon separation: surface engineering, molecular docking, and size exclusion. In addition, the prospects of MOF materials for hydrocarbon separation are discussed, including future directions of addressing the challenges (barriers) for MOF sorbents to be competitive in practical applications, such as adsorption capacity and selectivity, stability, regenerability, scalability and cost-effectiveness, and industrial implementation.

Received 2nd July 2023
Accepted 30th August 2023

DOI: 10.1039/d3ta03852a

rsc.li/materials-a

1. Introduction

Hydrocarbons such as ethylene (C_2H_4), propylene (C_3H_6), and xylenes are the most important feedstock materials in the petrochemical industry,[1] with an estimated value exceeding USD 307.58 billion by 2029.[2,3] High-purity hydrocarbons are essential for the downstream production of high-value-added chemical products;[4] yet current hydrocarbon separation technology is extremely energy-intensive with high energy penalties.[5] For example, cryogenic distillation coupled with high plate numbers and reflux ratios is often required in industrial separation processes to obtain high-purity hydrocarbons, resulting in associated equipment investment and energy consumption of up to 40–90% of the total process cost.[6,7] Therefore,

College of Chemistry and Materials Science, Guangdong Provincial Key Laboratory of Functional Supramolecular Coordination Materials and Applications, Jinan University, Guangzhou 510632, P. R. China. E-mail: weiganglu@jnu.edu.cn; danli@jnu.edu.cn

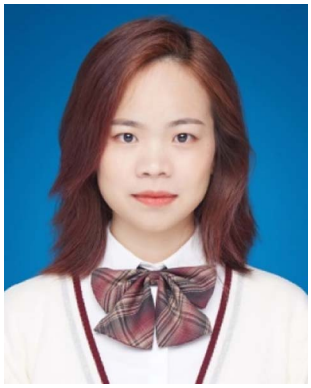

Xiao-Jing Xie joined Prof. Dan Li's group at Jinan University as a PhD student in 2021. She completed her B.S. degree at the College of Chemistry and Materials Science, Jinan University, in 2020. Her current research interests are the design and application of metal–organic frameworks for hydrocarbon separation.

Heng Zeng received his PhD degree in chemistry from Jinan University in 2022. His research work is focused on the development of multifunctional metal–organic frameworks and hydrogen-bonding organic frameworks for their applications in gas storage, separation, and sensors.

developing alternative separation technology for hydrocarbon purification with less energy consumption and environmental impact is of practical significance from academic research to industrial implementation.

Adsorption-based separation using porous materials has demonstrated great potential as an eco-friendly and energy-efficient technology, accounting for only 1/3 or less of the energy consumption of cryogenic distillation.[8,9] Meanwhile, adsorption-based separation has also shown its capability of enabling high separation selectivity, allowing for the better implementation of challenging separations. Traditional porous solids (*e.g.* zeolites[10] and carbon materials[11]) have been explored as adsorbents in the separation of hydrocarbons, for example, the removal of linear alkanes from their branched isomers with zeolite 5A.[12] However, because of their limited structural diversity and designability, zeolites appear to be inadequate for many other industrially demanding hydrocarbon separations.[13] To reduce the energy footprint of hydrocarbon separations, scientists and engineers in academia and industry are facing the opportunities and challenges of developing efficient adsorbents to overcome the trade-off between the adsorption capacity and separation coefficient.[14,15]

Metal–organic frameworks (MOFs),[16,17] also known as porous coordination polymers (PCPs), are a class of porous crystalline materials assembled from metal nodes/metal clusters (a.k.a. secondary building units, SBUs) and organic linkers. With the rapid advances in reticular chemistry and crystal engineering, researchers have gained deep insight into the directional stitching of diverse building blocks, paving the way for the design and construction of tailor-made MOF materials. Compared to traditional porous solids, MOF materials are known for their exceptional porosity (specific surface area up to 7000 $m^2 g^{-1}$) and diverse pore structures, which can be beneficial for sensing,[18] catalysis,[19] biomedicine,[20] separation,[21] and other relevant applications.[22] Particularly, MOF materials have shown enormous potential in the separation and purification of hydrocarbons owing to their ultrahigh surface area, tunable pore environment, and structural designability. One of the most notable features of MOFs is post-synthetic modification, which allows for the introduction of additional functionalities or active sites into the MOF structures, further enhancing their performance. Another notable feature of MOFs is their well-defined pore structures, which enables a better understanding in terms of structure–property relationships, and therefore, provides directions to further design MOF materials for higher adsorption selectivity. In addition, framework flexibility was observed in over 200 reported MOF materials, leading to many interesting and unexpected properties contingent upon the applied stimuli (*e.g.*, guest, temperature, pressure, light, electricity, *etc.*).[23–25]

Currently, the design and construction of MOF materials for hydrocarbon separation can be roughly categorized into the following three main strategies: surface engineering, molecular docking, and size exclusion (Fig. 1). Surface engineering is to install certain functional groups on the internal surface of MOF materials to distinguish gas molecules. For example, MOF materials with open metal sites tend to have a stronger binding affinity for olefin than for paraffin. Molecular docking is to build pockets/traps with matched dimensions and electrostatic potentials to preferentially accommodate specific guest molecules, not necessarily the smaller ones. Size exclusion is considered an ideal strategy for hydrocarbon separation, in which smaller molecules are adsorbed and larger ones are completely excluded, offering the highest separation coefficient among the three strategies. This perspective reviews the recent undertakings of the above three strategies in the development of MOF materials for hydrocarbon separation, focusing on their structure–property relationships. In addition, we discuss the prospects of MOF materials for hydrocarbon separation and the existing barriers to moving from academic research to industrial implementation.

Weigang Lu obtained his PhD in organic chemistry (2002) and stayed as a lecturer at Sun Yat-Sen University (2002–2005). After a visiting scholar stint at the Hong Kong University of Science & Technology (2005–2008), he joined Texas A&M University as an assistant research scientist in Prof. Hong-Cai Zhou's group (2008–2015). He started independent research as a research specialist at Fayetteville State University (2016–2018) and now he is a professor of chemistry at Jinan University (2018–Present). His research interest focuses on the rational design and synthesis of porous materials for energy-related applications.

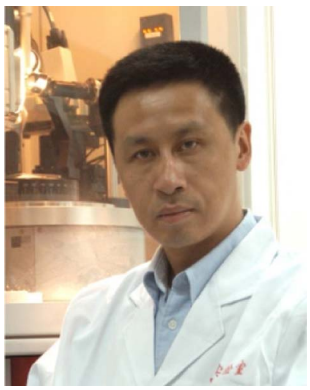

Dan Li received his BSc from Sun Yat-Sen University in 1984 and then worked at Shantou University. He pursued his PhD at The University of Hong Kong with Professor Chi-Ming Che during 1988–1993. Then he returned to Shantou University and became a Professor in 2001. He moved to Jinan University in Guangzhou in 2016. He is a recipient of the National Science Fund for Distinguished Young Scholars of China in 2008 and a Fellow of The Royal Society of Chemistry (FRSC) in 2014. His research interest is the design and fabrication of supramolecular coordination assemblies and their functions including photoluminescence, porosity and chirality. He has been serving as an Associate Editor of J. Mater. Chem. A and Mater. Adv. since mid-2022.

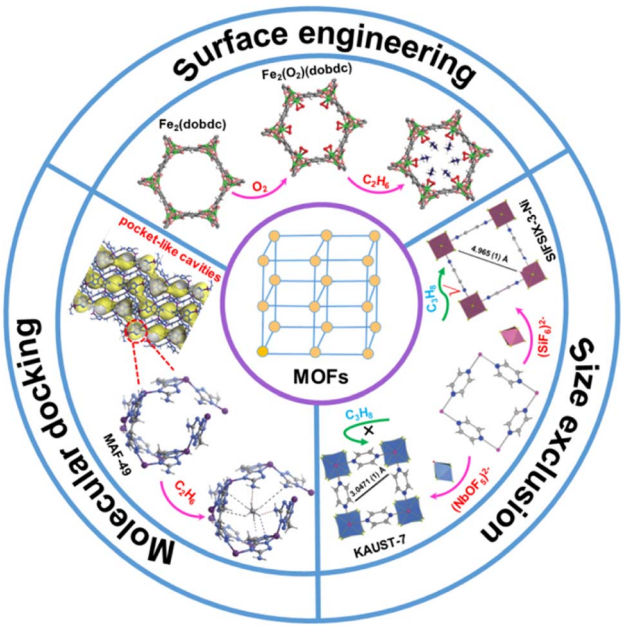

Fig. 1 Schematic diagram of the three main strategies for developing MOF materials for hydrocarbon separation. (Top) Reproduced from ref. 34 with permission from copyright 2018, The American Association for the Advancement of Science. (Bottom-left) Reproduced from ref. 46 with permission from copyright 2015, Springer Nature. (Bottom-right) Reproduced from ref. 59 with permission from copyright 2016, The American Association for the Advancement of Science.

2. Design strategies

2.1. Surface engineering

Surface engineering represents an intuitive and effective strategy in the study of MOF materials for hydrocarbon separation. The introduction of functional groups on the internal surface may endow MOF materials with polarized surfaces or electric field gradients to boost adsorbate–adsorbent interaction. Extensive research efforts have been devoted to rational surface engineering by the systematic installation of functional groups *via* reticular synthesis.

MOF materials with coordinatively unsaturated metal sites (open metal sites) can preferentially adsorb alkenes over alkanes through metal–π interaction and thus have attracted substantial attention for their use in olefin/paraffin separation. As early as 2002, Bülow Martin *et al.* first reported the separation of C_2H_4/C_2H_6 mixtures with $Cu_3(BTC)_2$ (HKUST-1), a landmark MOF material with Cu^{II} open metal sites on the axial positions of copper paddlewheel clusters.[26] Detailed theoretical calculations revealed that C_2H_4 is indeed preferentially adsorbed on the Cu^{II} open metal site *via* the metal–π interaction.[27] In 2012, Jeffrey R. Long *et al.* examined an iron-based MOF, Fe_2(dobdc) (dobdc: 2,5-dioxido-1,4-benzenedicarboxylate), because of its ability to separate C_2H_4/C_2H_6 and C_3H_6/C_3H_8 at 318 K.[28] Fe_2(dobdc) exhibited a strong affinity towards C_2H_2, C_2H_4, and C_3H_6, as evidenced by their steep adsorption curves at low pressures in the adsorption isotherms of these unsaturated hydrocarbons. Neutron powder diffraction (NPD) studies directly revealed that both C_2H_4 and C_3H_6 are bound to the Fe^{II} open metal sites in side-on mode, with Fe–C distances in the range from 2.42(2) to 2.60(2) Å, while the interactions of C_2H_6 and C_3H_8 with the Fe^{II} open metal sites are much weaker, as evidenced by the longer Fe–C distances (~3 Å) (Fig. 2a and b). Equilibrium adsorption experiments demonstrate that Fe_2(dobdc) exhibited large olefin adsorption capacities and high olefin/paraffin selectivities (up to 18 for C_2H_4/C_2H_6 and 15 for C_3H_6/C_3H_8) at 318 K. Breakthrough experiments confirmed that Fe_2(dobdc) is capable of separating an equimolar mixture of C_2H_4/C_2H_6 and C_3H_6/C_3H_8 at 1 bar and 318 K, affording olefins with >99% purity (Fig. 2c and d).

Since open metal sites can be used to reversibly bind olefin molecules *via* metal–π interaction, introducing high-density open metal sites is one of the most effective strategies for olefin/paraffin separation.[29–31] Most of the reported MOF materials can offer up to one accessible open metal site per metal center. In 2022, our group reported a microporous MOF (JNU-4) consisting of square-planar mononuclear Cu^{II} centers and tetrahedral organic linkers, allowing for two accessible binding sites per metal center for C_2H_2 molecules.[32] The adsorption isotherm of JNU-4 exhibited a steep adsorption curve at low pressures and an overall adsorption capacity of 222 $cm^3\ g^{-1}$ (9.91 mmol g^{-1}) at 298 K and 1 bar. Computational modeling studies revealed that C_2H_2 molecules preferentially occupy both sides of the square-planar metal centers. Breakthrough experiments demonstrated that JNU-4 is capable of achieving by far the largest C_2H_2 capture capacity (7.14 mmol g^{-1}) from an equimolar mixture of C_2H_2/CO_2, and fuel-grade C_2H_2 production (4.69 mmol g^{-1}, ≥98%) upon desorption.

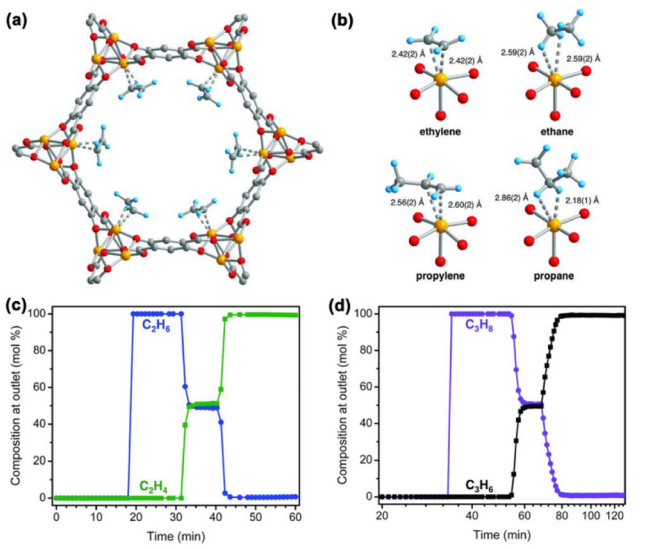

Fig. 2 (a) The structure of Fe_2(dobdc)·$2C_2D_4$ from neutron powder diffraction data, showing the strong metal–π interactions. (b) Views of the iron centers interacting with C_2D_4, C_2D_6, C_3D_6, and C_3D_8. Orange, red, gray, and blue spheres represent Fe, O, C, and D atoms, respectively. (c) and (d) Experimental breakthrough curves for equimolar C_2H_4/C_2H_6 and C_3H_6/C_3H_8 mixtures on Fe_2(dobdc). Reproduced from ref. 28 with permission from copyright 2012, The American Association for the Advancement of Science.

Despite having more accessible binding sites, most of the MOF materials used for hydrocarbon separation have rigid frameworks whose dimensions/pore sizes hardly change upon loading with guest molecules, resulting in a decrease in binding affinity once the strongest adsorption sites are occupied. The flexible MOFs with induced-fit behavior may adaptively match the sizes and shapes of the guest molecules, gradually enhancing the host–guest interaction. Meanwhile MOF materials constructed with infinite 1-periodic metal clusters are known for their exceptional stability. In 2019, our group reported the synthesis of a highly stable MOF (JNU-1) from the reaction of benzotriazole-5-carboxylic acid (H_2btca) and $Zn(NO_3)_2 \cdot 6H_2O$.[33] JNU-1 contains 1-periodic Zn clusters with high-density open metal sites oriented toward the one-dimensional (1D) diamond-shaped channels. More importantly, it exhibited an induced-fit adsorption behavior when exposed to C_2H_2 (Fig. 3). C_2H_2 adsorption isotherms displayed step-shaped adsorption curves at low pressures, which gradually disappeared with increasing temperature. Continuous C_2H_2 adsorption/desorption measurements confirmed the robust interaction with C_2H_2, and JNU-1 can only be fully regenerated under a high vacuum and a high temperature (393 K). *In situ* powder X-ray diffraction (PXRD) measurements implied that the JNU-1 framework can self-adaptively shrink in response to C_2H_2 (Fig. 3d), resulting in a rarely observed continuously increasing C_2H_2 binding affinity with C_2H_2 loading, as evidenced by the calculated C_2H_2 adsorption enthalpy (Q_{st}) (Fig. 3c). *In situ* single-crystal X-ray diffraction (SCXRD) and computational simulation revealed that C_2H_2 is initially bound by two unsaturated Zn metal sites *via* side-on metal–π interactions (Fig. 3a and b) and the channel size of JNU-1 along the *b* axis is eventually reduced from 12.7 to 10.8 Å, confirming the induced-fit behavior of JNU-1 upon C_2H_2 adsorption.

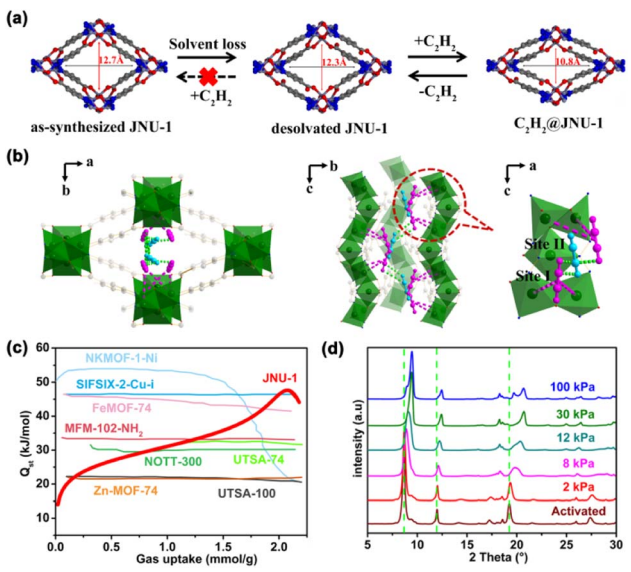

Fig. 3 (a) Schematic representation of the induced-fit behavior of JNU-1 upon C_2H_2 adsorption. (b) Single-crystal structure of C_2H_2@JNU-1 with C_2H_2 molecules being observed on the primary site (site I, pink) and the secondary site (site II, blue). (c) Comparison of the C_2H_2 adsorption enthalpy (Q_{st}) of JNU-1 and some selected MOFs. (d) *In situ* PXRD patterns of JNU-1 at different C_2H_2 concentrations. Reproduced from ref. 33 with permission from copyright 2019, John Wiley and Sons.

Although seemingly efficient, the olefin/paraffin separation relying on the open metal sites of MOF materials could be dramatically diminished under humid conditions due to their equally strong (if not more) binding affinity toward the water molecules. On the other hand, introducing polar functional groups with electronegative elements (*e.g.*, N, O, and F) has been widely explored as an alternative approach to facilitate the olefin/paraffin separation. Many MOFs have been explored for the separation of C_2H_6/C_2H_4 based on surface engineering strategies (Table 1). In 2018, inspired by natural metalloenzymes and synthetic compounds for alkane C–H activation, including metal–peroxo, metal–hydroperoxo, and metal–oxo species, Chen *et al.* reported iron oxidation of the MOF material Fe_2(dobdc),[34] and the obtained $Fe_2(O_2)$(dobdc) exhibited a preferential binding of C_2H_6 over C_2H_4 and the highest C_2H_6/C_2H_4 separation coefficient (4.4) (Fig. 4a). Single-component adsorption isotherm results showed that the C_2H_6 adsorption capacity of $Fe_2(O_2)$(dobdc) reached 74.3 $cm^3\ g^{-1}$ (3.32 mmol g^{-1}) (Fig. 4b), realizing a reversed C_2H_6/C_2H_4 adsorption behaviour as opposed to pristine Fe_2(dobdc). High-resolution neutron powder diffraction (NPD) measurements revealed that C_2D_6 preferentially binds the peroxo site through a C–D···O interaction (D···O, ~2.17 to 2.22 Å) (Fig. 4a), with a distance much shorter than the sum of the van der Waals (vdW) radii of the oxygen (1.52 Å) and hydrogen (1.20 Å) atoms. The C_2H_4/C_2H_6 (50/50) breakthrough results confirmed that $Fe_2(O_2)$(dobdc) is capable of directly producing 0.79 mmol g^{-1} of C_2H_4 with ≥99.99% purity in a single breakthrough operation (Fig. 4c).

The introduced polar functional groups, however, may also interact with water molecules, which could significantly affect their separation potential under humid conditions. For example, the $Fe_2(O_2)$(dobdc) material must be handled inside a glove box. Recent studies show that nonpolar environments can block moisture from entering inside the frameworks, thus maintaining the C_2H_4/C_2H_6 separation potential even under humid conditions. Considering that the polarizability of alkanes is higher than that of alkenes (C_2H_4: 42.52×10^{-25} cm^3, C_2H_6: 44.7×10^{-25} cm^3, C_3H_6: 62.6×10^{-25} cm^3, and C_3H_8: 63.7×10^{-25} cm^3),[35] introducing nonpolar functional groups (*e.g.*, –methyl, –naphthalene, and –anthracene) on the pore surface could provide a substantial energetic contribution to the preferential adsorption of alkanes over alkenes.[36–43] In 2018, Chen *et al.* reported two isoreticular ultramicroporous MOF materials, $Cu(ina)_2$ (Hina = isonicotinic acid) and $Cu(Qc)_2$ (HQc = quinolone-5-carboxylic acid), for C_2H_6/C_2H_4 separation (Fig. 5a and b).[44] The pore surfaces of both MOF materials are decorated with aromatic rings, which favour the binding of more polarizable C_2H_6 over C_2H_4. From a structural point of view, $Cu(Qc)_2$ has a smaller pore aperture and a larger aromatic π system than $Cu(ina)_2$, which endows $Cu(Qc)_2$ with further improved C_2H_6/C_2H_4 separation performance as a C_2H_6-selective adsorbent. As expected, C_2H_6 and C_2H_4 adsorption isotherms at 298 K and 1 bar on $Cu(Qc)_2$ can reach up to 60.0 $cm^3\ cm^{-3}$ (1.85 mmol g^{-1})

Table 1 Some selected MOFs for C_2H_6/C_2H_4 separation based on the surface engineering strategy

Materials	T (K)	C_2H_6/C_2H_4 uptake (mmol g^{-1}, 1 bar)	IAST selectivity (C_2H_6/C_2H_4, 50/50)	Interaction	Ref.
NKMOF-8-Br	298	4.22/3.67	2.65	C–H···π	46
NKMOF-8-Me	298	4.82/4.67	1.88	C–H···π	46
$Cu(Qc)_2$	298	1.85/0.78	3.4	C–H···π	44
IRMOF-8	298	3.6/2.75	1.6	C–H···π	39
$Fe_2(O_2)$(dobdc)	298	3.4/2.6	4.4	C–H···O	34
MUF-15	293	4.69/4.15	1.96	C–H···π	38
TJT-100	298	3.66/3.4	1.2	C–H···O	47
$Ni(IN)_2$	298	3.05/0.8	2.44	C–H···π	37
AzoleTh-1	298	4.47/3.62	1.46	C–H···π	43
FJI-H11-Me(des)	298	2.59/2.05	2.09	C–H···O/π	45
1a	298	3.63/3.28	2.15	C–H···O/π/N	41
Tb-MOF-76(NH_2)	298	3.27/2.97	2.05	C–H···O/π/N	48
UiO-67-$(NH_2)_2$	296	5.32/4.32	1.7	C–H···O/π/N	49
Zn-atz-oba	298	2.1/2	1.27	C–H···N	50

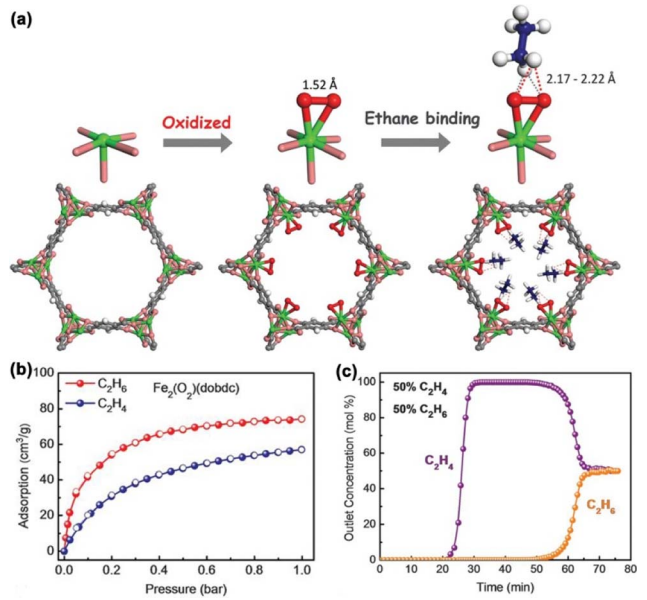

Fig. 4 (a) Structure of $Fe_2(O_2)$(dobdc) and its interaction with C_2D_6 determined from neutron powder diffraction (NPD) studies. (b) C_2H_6 and C_2H_4 single-component adsorption isotherms of $Fe_2(O_2)$(dobdc) at 298 K. (c) Experimental column breakthrough curves of $Fe_2(O_2)$(dobdc) for C_2H_4/C_2H_6 (50/50) mixtures at 298 K. Reproduced from ref. 34 with permission from copyright 2018, The American Association for the Advancement of Science.

and 25.3 $cm^3\ cm^{-3}$ (0.78 mmol g^{-1}), respectively (Fig. 5c), resulting in a superior C_2H_6/C_2H_4 uptake ratio of 237%. This value is much higher than that of its isoreticular analog $Cu(ina)_2$ (105%). High-resolution neutron powder diffraction (NPD) analyses of the C_2D_6-loaded $Cu(Qc)_2$ revealed that the C_2D_6 molecule is located in a rhombic cavity formed by aromatic rings of ligands from the same layered network *via* multiple C–D···π interactions (Fig. 5d and e). The breakthrough experimental result for an equimolar C_2H_4/C_2H_6 mixture demonstrated a complete separation of C_2H_4 from the C_2H_6/C_2H_4 mixture, affording a C_2H_4 productivity of 587 mmol L^{-1} (C_2H_4/adsorbent) (Fig. 5f). This strategy was also illustrated in the MOF material FJI-H11-Me(des),[45] and the accessible surface of FJI-H11-Me(des) is decorated with aromatic rings and alkyl groups of the ligands, resulting in a preferential C_2H_6 adsorption over C_2H_4. The adsorption capacity can reach up to 57.97 $cm^3\ g^{-1}$ (2.59 mmol g^{-1}) and 46.65 $cm^3\ g^{-1}$ (2.08 mmol g^{-1}) for C_2H_6 and C_2H_4, respectively, at 298 K and 1 bar. In addition, it is worth noting that the separation performance of FJI-H11-Me(des) was not affected even under high relative humidity (RH) due to its hydrophobicity.

2.2. Molecular docking

Molecular docking is known in biological processes for recognizing and placing specific molecules at the receptor sites of proteins. For some MOF materials, their structures can be characterized by pocket-like cavities, which may preferentially accommodate guest molecules of matching sizes and shapes, not necessarily the smaller ones. The rational design of

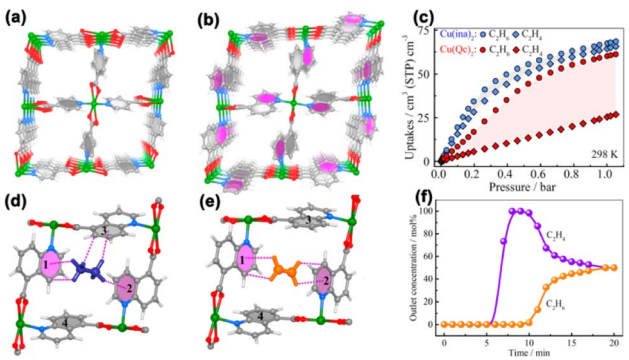

Fig. 5 (a) and (b) Crystal structures of $Cu(ina)_2$ and $Cu(Qc)_2$. (c) Adsorption isotherms of C_2H_6 and C_2H_4 on $Cu(ina)_2$ and $Cu(Qc)_2$ at 298 K. (d) and (e) Neutron diffraction crystal structures of $[Cu(Qc)_2]$@C_2D_6 and $[Cu(Qc)_2]$@C_2D_4. (f) Experimental breakthrough curves of $Cu(Qc)_2$ for an equimolar C_2H_6/C_2H_4 mixture at 298 K and 1.0 bar. Reproduced from ref. 44 with permission from copyright 2018, American Chemical Society.

molecular pockets or traps can endow MOFs with great potential for hydrocarbon separation.

In 2015, Chen and Zhang *et al.* reported a microporous MOF, MAF-49, featuring 1D zigzag channels decorated with multiple nitrogen-containing groups (Fig. 6a).[51] The single-component gas adsorption isotherms of MAF-49 showed a higher uptake of C_2H_6 than C_2H_4 at 316 K (Fig. 6b) and an exceptionally high C_2H_6/C_2H_4 selectivity of 9. *In situ* SCXRD and computational simulation revealed that C_2H_6 forms six C–H···N interactions within the pockets on the channels, while C_2H_4 forms four C–H···N interactions (Fig. 6c and d). The excellent C_2H_6/C_2H_4 separation potential of MAF-49 was verified by breakthrough experiments on a C_2H_6/C_2H_4 mixed gas. This work has successfully demonstrated that the introduction of multiple hydrogen-bonding acceptors on the pore surface of molecular pockets is an effective strategy to discriminate paraffin from olefin. It should be pointed out that, despite having high C_2H_6/C_2H_4 selectivity, the molecule-pocket-based MAF-49 exhibited a limited adsorption capacity of C_2H_6 (1.7 mmol g^{-1}), probably because every molecular pocket can only accommodate one molecule. Furthermore, considering its highly electronegative environment of the molecular pocket, MAF-49 may not be able to maintain its C_2H_6/C_2H_4 separation capacity under humid conditions due to the competition of water molecules for the adsorption sites.

In 2019, our group reported a microporous MOF (JNU-2)[52] with cage-like cavities interconnected through tailored apertures (Fig. 7a). The aperture size of 3.7 Å is in the domain of the kinetic diameters of C_2H_4 and C_2H_6 molecules. Indeed, C_2H_4 and C_2H_6 adsorption isotherms showed that JNU-2 exhibited a preferential binding of C_2H_6 over C_2H_4. The adsorption capacity of C_2H_6 can reach up to 4.19 mmol g^{-1} at 298 K and 1 bar (Fig. 7b), indicating that the large cavities of JNU-2 can be translated into large adsorption capacity, and this value is higher than that of most of the benchmark MOF materials. Molecular modeling studies revealed that C_2H_6 forms four weak hydrogen bonds with oxygen atoms at the aperture, while C_2H_4 forms only two weak hydrogen bonds (Fig. 7c and d).

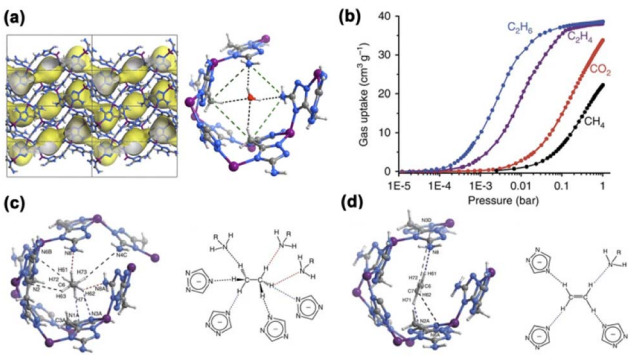

Fig. 6 (a) Crystal structure of MAF-49, showing a water molecule in the molecular pocket. (b) Single-component adsorption isotherms of C_2H_6, C_2H_4, C_2H_2, and CO_2 on MAF-49 at 316 K. Crystal structure of (c) C_2H_6@MAF-49 and (d) C_2H_4@MAF-49, highlighting the multiple binding interactions. Reproduced from ref. 51 with permission from copyright 2015, Springer Nature.

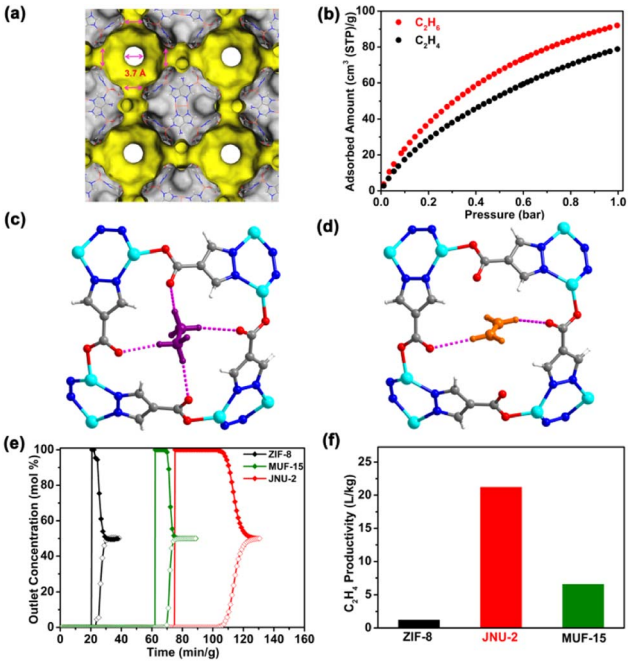

Fig. 7 (a) Connolly surface representation of the cage-interconnected structure of JNU-2. (b) Single-component adsorption isotherms of C_2H_6 and C_2H_4 on JNU-2 at 298 K. Host–guest interactions of (c) C_2H_6 and (d) C_2H_4 with JNU-2 at the aperture. (e) Comparison of the breakthrough curves of JNU-2 and other MOF materials for an equimolar C_2H_6/C_2H_4 mixture at a flow rate of 1.0 mL min^{-1} and 298 K. (f) Comparison of C_2H_4 productivity estimated from the breakthrough curves of ZIF-8, MUF-15, and JNU-2. Reproduced from ref. 52 with permission from copyright 2019, American Chemical Society.

Breakthrough experiments under dry conditions showed that about 21.2 L of C_2H_4 with over 99.99% purity could be retrieved from a C_2H_6/C_2H_4 (50/50) mixture for 1 kg of JNU-2, which is higher than most of the benchmark C_2H_6-selective adsorbents, including MUF-15 (6.6 L kg^{-1}) and ZIF-8 (1.2 L kg^{-1}) (Fig. 7e and f). Furthermore, breakthrough experiments under humid conditions demonstrated that JNU-2 maintained its exceptional separation potential for C_2H_6/C_2H_4 mixtures. Overall, JNU-2 can achieve both large C_2H_6 adsorption capacity and a high C_2H_6/C_2H_4 separation coefficient even under humid conditions due to its cage-interconnected structure and balanced hydrophilicity/hydrophobicity.[53] The apertures connecting the cages function as screening sites for C_2H_6 molecules to preferentially go through, while the internal cavities provide a large surface for adsorption capacity. By constructing MOF materials with large cavities interconnected by tailor-made apertures, this work has successfully exemplified a promising strategy for hydrocarbon separation with balanced adsorption capacity and separation coefficient.

Considering that the molecule pockets/traps are located right on the diffusion pathways for most MOF materials, the adsorption equilibrium could be difficult to reach as the matched molecules have to pass through many apertures, leading to slow adsorption/desorption kinetics and thus less energy efficiency. In 2021, our group reported an orthogonal-

array dynamic molecular sieving material, JNU-3a, enabling both large separation capacity and fast adsorption–desorption kinetics for C_3H_6/C_3H_8 separation.[54] SCXRD analysis revealed that JNU-3a featured a 1D channel with orthogonal-array molecular pockets on both sides opening to the channel through 'gourd-shaped' apertures. The size of the aperture is approximately 3.7 Å, which seemed impossible for C_3H_6 (4.0 Å) and C_3H_8 (4.3 Å) to go through (Fig. 8a–c). Yet, *in situ* SCXRD studies on gas@JNU-3a observed tilting and rotation of the aromatic ring on the organic linker, facilitating the guest molecules such as C_3H_6 and C_3H_8 to open the 'gourd-shaped' apertures and enter into the pockets (Fig. 8d). As such, both C_3H_6 and C_3H_8 displayed stepwise adsorption, and the gate-opening pressure of C_3H_8 is about 0.52 bar at 303 K, approximately five times higher than that of C_3H_6, offering a high selectivity of C_3H_6 over C_3H_8 (Fig. 8e). Breakthrough experiments under dry conditions demonstrated that 34.2 L of C_3H_6 with over 99.5% purity could be obtained from an equimolar C_3H_6/C_3H_8 mixture at a flow rate of 1.0 mL min^{-1} for 1 kg of JNU-3a in a single adsorption/desorption cycle. Moreover, 53.5 L and 44.9 L of C_3H_6 with over 99.5% purity could be obtained from an equimolar C_3H_6/C_3H_8 mixture for 1 kg of JNU-3a under 0% RH and 50% RH conditions, respectively, at a flow rate of 6.0 mL min^{-1}. Owing to the orthogonal-array dynamic molecular sieving mechanism, the diffusion kinetics of C_3H_6 and C_3H_8 on JNU-3a are at least one order of magnitude faster than those of the two reported best-performing sieving materials (KAUST-7 and Y-abtc) for C_3H_6/C_3H_8 mixtures. JNU-3a represented next-generation molecular sieving materials with intrinsically fast adsorption–desorption kinetics, applicable not only to hydrocarbon separation but also to other adsorptive separations.

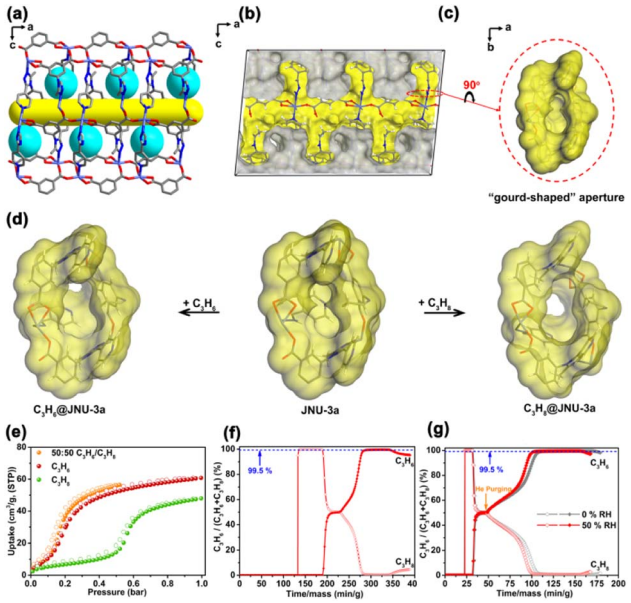

Fig. 8 (a) Pore structure of JNU-3 viewed along the *b* axis showing the molecular pockets (turquoise) and the 1D channel (yellow). (b) Cross-sectional view of the Connolly surface of the void in (a), where a probe radius of 0.8 Å was used to visualize the molecular pockets opening to the 1D channel. (c) Close-up view of the "gourd-shaped" aperture connecting the pocket to the channel. (d) Connolly surface of the "gourd-shaped" apertures in C_3H_6@JNU-3a and C_3H_8@JNU-3a. (e) Single-component adsorption/desorption isotherms of C_3H_6, C_3H_8, and C_3H_6/C_3H_8 (50 : 50) on JNU-3a at 303 K. (f) Breakthrough curves of an equimolar mixture of C_3H_6/C_3H_8 (1.0 mL min^{-1}) on JNU-3a, followed by desorption curves under helium gas (10.0 mL min^{-1}) sweeping at 303 K. (g) Breakthrough curves of an equimolar mixture of C_3H_6/C_3H_8 (6.0 mL min^{-1}) on JNU-3a under 0% RH and 50% RH conditions, followed by desorption curves under helium gas (10.0 mL min^{-1}) sweeping at 303 K. Reproduced from ref. 54 with permission from copyright 2021, Springer Nature.

2.3. Size exclusion

Size exclusion is considered to be one of the most promising separation strategies for hydrocarbon separation due to its potential to completely block larger molecules and therefore provide an infinite selectivity.[55–58] In addition, the rigid molecular sieving MOF materials can effectively avoid the co-adsorption of analogous alkanes that are commonly observed in MOF materials with open metal sites. However, the molecular-size difference is 0.42 Å for C_3H_8 and C_3H_6 and only 0.28 Å for C_2H_6 and C_2H_4. It is challenging to design and construct MOF materials with the right aperture sizes as molecular sieves for targeted hydrocarbon separation.

In 2018, Chen *et al.* reported the synthesis of a microporous MOF material, $Ca(C_4O_4)(H_2O)$ (UTSA-280), from calcium nitrate and squaric acid under mild aqueous conditions. UTSA-280 possesses a rigid 1D channel with an aperture large enough for C_2H_4 inclusion but not for C_2H_6 (Fig. 9a and b).[59] The cross-sectional area of the rigid 1D channel is about 14.4 $Å^2$, which falls between the minimum cross-sectional areas of C_2H_4 (13.7

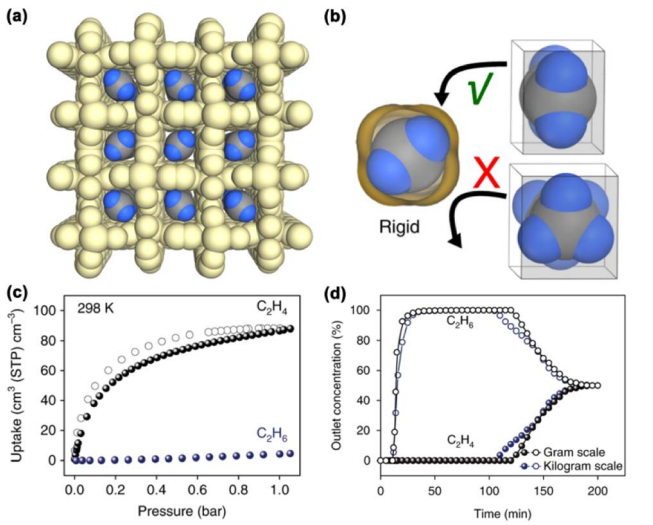

Fig. 9 (a) View of the crystal structure and packing diagram of C_2H_4@UTSA-280. (b) Schematic illustration of size/shape sieving based on the minimum cross-sectional area of C_2H_4 and C_2H_6 molecules. (c) Single-component adsorption/desorption isotherms of C_2H_4 and C_2H_6 at 298 K. (d) Comparison of experimental breakthrough curves for a 50/50 C_2H_4/C_2H_6 mixture on UTSA-280 synthesized on different scales. Reproduced from ref. 59 with permission from copyright 2018, Springer Nature.

Å^2) and C_2H_6 (15.5 Å^2). C_2H_6 adsorption isotherms confirmed that the adsorption of C_2H_6 at 298 K and 1 bar is a mere 0.098 mmol g^{-1}, indicating the complete blocking of C_2H_6. On the other hand, the adsorption of C_2H_4 could reach up to 2.5 mmol g^{-1} under similar conditions (Fig. 9c). UTSA-280 set the record for the C_2H_4/C_2H_6 separation coefficient (>10 000), which is orders of magnitude higher than those of previously reported MOF materials, such as NOTT-300 (48.7) and Mg-gallate (52). SCXRD studies of the C_2H_4-loaded UTSA-280 coupled with density functional theory (DFT) calculations revealed that the C=C axis of the C_2H_4 molecule is aligned along the channel, interacting with the surroundings through C–H···O hydrogen bonding, π···π stacking, and vdW interactions. In contrast, C_2H_6 cannot enter into the channels because of its slightly oversized molecular dimension. The capture capacity of C_2H_4 can reach up to 1.86 mmol g^{-1} from an equimolar C_2H_4/C_2H_6 mixture, which is slightly lower than the equilibrium adsorption capacity of UTSA-280 at 0.5 bar (2.05 mol kg^{-1}). Moreover, UTSA-280 can be synthesized on a kilogram scale under environmentally friendly conditions, and the obtained material maintains excellent separation performance (Fig. 9d).

In the same year, Ren *et al.* reported a family of gallate-based MOF materials, M-gallate (M = Ni, Mg, Co), with interconnected zigzag channels (3.47 × 4.85, 3.56 × 4.84, and 3.69 × 4.95 Å^2 for Ni, Mg, Co-gallate, respectively),[60] which are between the molecular sizes of C_2H_6 (3.81 × 4.08 × 4.82 Å^3) and C_2H_4 (3.28 × 4.18 × 4.84 Å^3). Adsorption isotherms revealed that all M-gallate adsorbed only negligible amounts of C_2H_6 (<0.31 mmol g^{-1}) at 298 K up to 1 bar, indicating that C_2H_6 could be excluded from entering the pore channels. Experimental breakthrough tests for an equimolar C_2H_4/C_2H_6 mixture indicated that C_2H_6 was eluted through the packed column quickly and high-purity C_2H_4 could be obtained upon desorption. Neutron powder diffraction (NPD) experiments confirmed the adsorption site of C_2D_4 in Mg-gallate (Fig. 10). However, it should be pointed out that, in both cases, desorption is required in order to obtain C_2H_4, and its purity could be lower than expected due to the dead space in the packed column.

By contrast, the design and construction of MOF materials as molecular sieves for C_3H_6/C_3H_8 separation are more challenging due to their increased molecular flexibility.[61–63] Eddaoudi *et al.* reported the assembly of a fluorinated MOF, NbOFFIVE-1-Ni (KAUST-7),[64] with $(NbOF_5)^{2-}$ as pillars interconnecting the Ni(II)–pyrazine square-grid layers. The resulting 1D channel enables the complete molecular exclusion of C_3H_8 from C_3H_6. Compared to $(SiF_6)^{2-}$-pillared isomer SIFSIX-3-Ni, $(NbOF_5)^{2-}$ is a relatively larger spacer, leading to shorter C–H···F interaction distances between the anionic pillar and pyrazine, which hinders the rotation of the pyrazine ligand and reduces the pore aperture from 4.75 to 3.04 Å (Fig. 10a and b). Gas adsorption data indicated that the reduced pore size of KAUST-7 can still allow C_3H_6 to diffuse into the channels, but not C_3H_8. The adsorption profile of an equimolar C_3H_6/C_3H_8 mixture is in good agreement with that of pure C_3H_6 (Fig. 11c). Furthermore, both calorimetric and gravimetric measurements were carried out, and an almost negligible heat of adsorption of

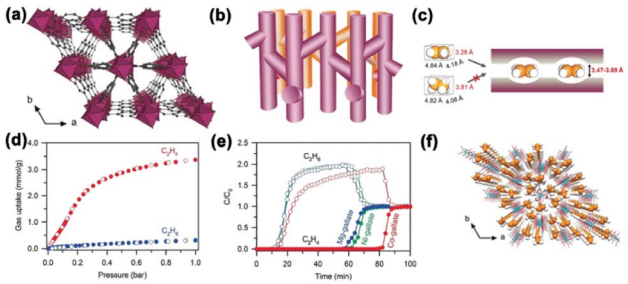

Fig. 10 (a) Perspective view of M-gallate along the *c*-axis showing a triangular main channel and regular branching channels abutting the main channel. (b) The zigzag channels of M-gallate. (c) Schematic diagram of M-gallate for C_2H_4/C_2H_6 separation. (d) Gas sorption isotherms of C_2H_4 (red) and C_2H_6 (blue) in Co-gallate at 298 K. (e) Experimental breakthrough curves at 273 K for M-gallate C_2H_4/C_2H_6 (50/50 mixture) separation with a flow rate of 0.5 mL min^{-1}. (f) Neutron diffraction crystal structure of Mg-gallate $0.485C_2D_4$ at 200 K. Reproduced from ref. 60 with permission from copyright 2018, John Wiley and Sons.

C_3H_8 was observed, confirming the molecular exclusion of C_3H_8. Breakthrough experiments were performed for an equimolar C_3H_6/C_3H_8 mixture to further confirm the separation potential of KAUST-7 (Fig. 11d). In addition, a number of custom-made frameworks have been designed for C_3H_6/C_3H_8 separation by precisely adjusting the pore size around 4.3–4.7 Å, from which the large C_3H_8 molecule can be excluded (Table 2). For example, Li and co-workers reported a microporous metal–

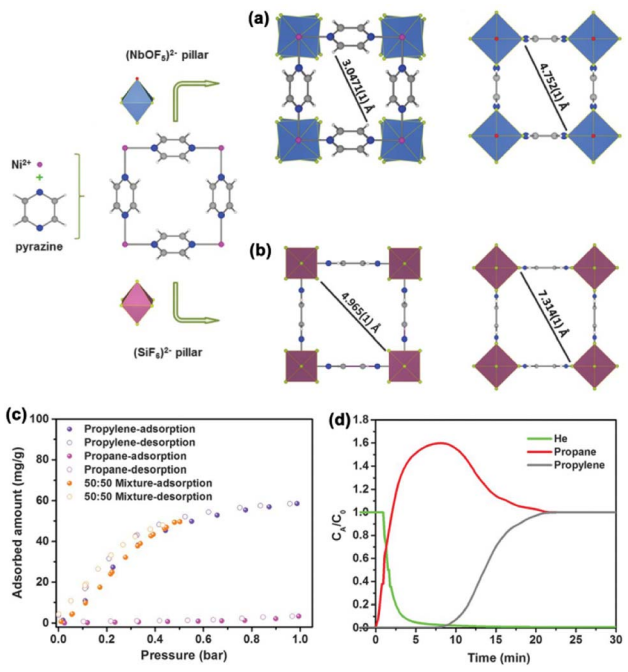

Fig. 11 Comparison of the building block arrangement of (a) KAUST-7 and (b) SIFSIX-3-Ni. (c) Adsorption isotherms of C_3H_6, C_3H_8, and an equimolar mixture of C_3H_6/C_3H_8 on KAUST-7 at 298 K. (d) Breakthrough curves for an equimolar C_3H_6/C_3H_8 mixture on KAUST-7 at 298 K. Reproduced from ref. 64 with permission from copyright 2016, The American Association for the Advancement of Science.

Table 2 A list of selected MOFs for separation of C_3H_6/C_3H_8 based on size exclusion

Materials	T (K)	C_3H_6 uptake (mmol g^{-1}, 1 bar)	C_3H_8 uptake (mmol g^{-1}, 1 bar)	Ref.
Co-gallate	298	1.79	0.14	67
HIAM-301	298	3.16	<0.3	62
KAUST-7	298	1.41	0.04	64
Y-bptc	298	1.95	0	65
UTSA-400	298	1.84	0.05	68
Y-dbai	298	2.57	0.1	69

organic framework $Y_6(OH)_8(abtc)_3(H_2O)_6(DMA)_2$ (Y-abtc). Benefiting from the optimal pore window size, Y-abtc can exclusively adsorb C_3H_6 with fast kinetics at ambient temperature.[65,66] Breakthrough measurements confirmed that polymer-grade propylene can be produced with a purity of 99.5% from a mixture of C_3H_6/C_3H_8 (5/95, v/v).

3. Conclusion and outlook

MOF materials are some of the most promising porous solids for adsorption applications due to their exceptional structural diversity, tunable pore dimension, and easy surface functionalization. This perspective summarizes the latest progress in the development of MOF materials for the selective adsorption of hydrocarbons, and three main strategies to design MOF materials for hydrocarbon separation: (1) surface engineering, installing functional groups on the pore surface to discriminate one hydrocarbon molecule from the others; (2) molecular docking, building molecular pockets to selectively trap guest molecules of particular sizes and shapes; (3) size exclusion, tuning the pore apertures precisely for the inclusion of only small-sized molecules.

The detailed MOF structures and their dynamic interactions with hydrocarbon molecules are critical to their performance in hydrocarbon separation. An in-depth understanding of the structure–property relationship can guide future MOF research in constructing specific structures and functions for the targeted separation. With the rapid development of *in situ* characterization techniques, it is now possible to study the dynamic interactions between the hosts (MOFs) and guests (gas molecules) at the molecular level. For example, *in situ* X-ray diffraction (XRD) or neutron diffraction allows researchers to see how the MOF structures are affected by the changes in temperatures, pressures, or gas compositions, providing insight into their stability, phase transitions, and host–guest interactions. *In situ* spectroscopy techniques such as FT-IR, Raman, and UV-vis can supply information about the electronic and vibrational properties of the MOF materials upon the inclusion of guest molecules, revealing the dynamic mechanisms of the adsorption/desorption processes. *In situ* microscopy and imaging techniques, such as transmission electron microscopy (TEM) coupled with gas adsorption, can produce high-resolution images with information on the distribution and location of guest molecules within the MOF materials. Computational methods, such as density functional theory (DFT), molecular dynamics (MD), and Monte Carlo simulations, can be used to calculate the binding energies, host–guest interactions, and dynamics of guest molecules within the MOF frameworks.

Currently, the study of MOF materials for separation applications is still largely in the lab stage. Achieving large adsorption capacity and high separation selectivity simultaneously seems to be a common goal for scientists and engineers in the development of MOF materials. For MOF sorbents to be competitive with conventional cryogenic processes for separations, there are also other challenges (barriers) that need to be addressed, including stability, regenerability, scalability and cost-effectiveness, and industrial implementation. An overall performance in these aspects would be ideal for the MOF sorbents. As for the future directions, we believe that these barriers these should be addressed collectively instead of individually.

(1) Adsorption capacity and selectivity: one of the promising strategies to balance selectivity and adsorption capacity for hydrocarbon separation is designing MOFs with large cavities interconnected by tailor-made apertures.[70–73]

(2) Stability: future research should focus on the development of robust and stable MOFs,[74] such as the design of high-valency metal–carboxylate frameworks and low-valency metal–azolate frameworks.[75]

(3) Regenerability: understanding adsorption/desorption mechanisms in MOFs is critical to developing effective regeneration techniques. By studying the interactions between the hydrocarbon molecules and the MOF structure at the molecular level, researchers can identify optimal conditions and methods for efficient desorption.

(4) Scalability and cost-effectiveness: the current practice of synthesizing MOF materials typically involves high-boiling-point solvents, which is not only costly but also environmentally unfriendly. More effort should be put into selecting inexpensive ligands and metal salts for water-mediated or non-mediated synthesis. Meanwhile, researchers should also explore scalable synthesis techniques, including continuous flow processes and microwave-assisted methods.

(5) Industrial implementation: bridging the gap between laboratory-scale research and industrial-scale applications is crucial. Collaboration between researchers, industry partners, and policy-makers can facilitate the deployment of MOF-based separation technologies in real-world settings.

Industrial crude hydrocarbon products often contain a variety of impurities, which may complicate the purification process. For example, if we intend to remove two or more components, they would inevitably compete for the adsorption

sites on the diffusion channels of the MOF materials, and one of them could be quickly pushed out, resulting in less efficient separation. Meanwhile, the desired component may not necessarily be the largest or smallest in terms of size; the one-step separation of medium-sized molecules is a significant challenge with tremendous implications for hydrocarbon separation, which may be achievable through the cooperative action of thermodynamics and kinetics. Different separation scenarios require MOF materials with different pores/channels and functions. Given the tunability of MOF structures in their pore dimensions and surface chemistry, adsorptive separation with MOF materials may indeed hold promise as an innovative technology for hydrocarbon separation, with the potential to replace the current energy-intensive practices.

Conflicts of interest

There are no conflicts to declare.

Acknowledgements

This work was financially supported by the National Natural Science Foundation of China (No. 21731002, 21975104, 22271120, 22301102, and 22150004), Guangdong Basic and Applied Basic Research Foundation (2023A1515010952), Innovation Team Project in Guangdong Colleges and Universities (2021KCXTD009), and National Postdoctoral Program for Innovative Talent (BX20220132).

Notes and references

1 D. S. Sholl and R. P. Lively, *Nature*, 2016, **532**, 435–437.
2 **https://www.databridgemarketresearch.com/reports/global-propylene-market**.
3 D. J. Safarik and R. B. Eldridge, *Ind. Eng. Chem. Res.*, 1998, **37**, 2571–2581.
4 S. M. Sadrameli, *Fuel*, 2015, **140**, 102–115.
5 S. Kitagawa, *Angew. Chem., Int. Ed.*, 2015, **54**, 10686–10687.
6 E. Worrell, D. Phylipsen, D. Einstein and N. Martin, *Energy Use and Energy Intensity of the U.S. Chemical Industry*, Lawrence Berkeley National Laboratory, Berkeley, CA, 2000.
7 S. Chu, Y. Cui and N. Liu, *Nat. Mater.*, 2017, **16**, 16–22.
8 H. Li, K. Wang, Y. Sun, C. T. Lollar, J. Li and H.-C. Zhou, *Mater. Today*, 2018, **21**, 108–121.
9 J. Kim, L. C. Lin, R. L. Martin, J. A. Swisher, M. Haranczyk and B. Smit, *Langmuir*, 2012, **28**, 11914–11919.
10 P. J. Bereciartua, Á. Cantín, A. Corma, J. L. Jordá, M. Palomino, F. Rey, S. Valencia, E. W. Corcoran Jr, P. Kortunov, P. I. Ravikovitch, A. Burton, C. Yoon, Y. Wang, C. Paur, J. Guzman, A. R. Bishop and G. L. Casty, *Science*, 2017, **358**, 1068–1071.
11 B.-U. Choi, D.-K. Choi, Y.-W. Lee, B.-K. Lee and S.-H. Kim, *J. Chem. Eng. Data*, 2003, **48**, 603–607.
12 Q. Gong, L. Yu, J. Ding, S. Zhang, Y. Bo, K. Chi, H. Wang, Q. Xia, S. He and J. Li, *Sep. Purif. Technol.*, 2022, **294**, 121219.
13 M. Hartmann, A. G. Machoke and W. Schwieger, *Chem. Soc. Rev.*, 2016, **45**, 3313–3330.
14 W. G. Cui, T. L. Hu and X. H. Bu, *Adv. Mater.*, 2020, **32**, 1806445.
15 Z. Bao, G. Chang, H. Xing, R. Krishna, Q. Ren and B. Chen, *Energy Environ. Sci.*, 2016, **9**, 3612–3641.
16 H. Furukawa, K. E Cordova, M. O'Keeffe and O. M. Yaghi, *Science*, 2013, **341**, 1230444.
17 W.-X. Zhang, P.-Q. Liao, R.-B. Lin, Y.-S. Wei, M.-H. Zeng and X.-M. Chen, *Coord. Chem. Rev.*, 2015, **293**, 263–278.
18 E. A. Dolgopolova, A. M. Rice, C. R. Martin and N. B. Shustova, *Chem. Soc. Rev.*, 2018, **47**, 4710–4728.
19 W. G. Cui, G. Y. Zhang, T. L. Hu and X. H. Bu, *Coord. Chem. Rev.*, 2019, **387**, 79–120.
20 M. Giménez-Marqués, T. Hidalgo, C. Serre and P. Horcajada, *Coord. Chem. Rev.*, 2016, **307**, 342–360.
21 X. Zhao, Y. Wang, D. S. Li, X. Bu and P. Feng, *Adv. Mater.*, 2018, **30**, 1705189.
22 K. Adil, Y. Belmabkhout, R. S. Pillai, A. Cadiau, P. M. Bhatt, A. H. Assen, G. Maurin and M. Eddaoudi, *Chem. Soc. Rev.*, 2017, **46**, 3402–3430.
23 J. P. Zhang, H. L. Zhou, D. D. Zhou, P. Q. Liao and X.-M. Chen, *Natl. Sci. Rev.*, 2018, **5**, 907–919.
24 G. Fereyand and C. Serre, *Chem. Soc. Rev.*, 2009, **38**, 1380–1399.
25 Q. Chen, S. Xian, X. Dong, Y. Liu, H. Wang, D. H. Olson, L. J. Williams, Y. Han, X.-H. Bu and J. Li, *Angew. Chem., Int. Ed.*, 2021, **133**, 10687–10691.
26 Q. M. Wang, D. M. Shen, M. Bülow, M. L. Lau, S. G. Deng, F. R. Fitch, N. O. Lemcoff and J. Semanscin, *Microporous Mesoporous Mater.*, 2002, **55**, 217–230.
27 W. You, Y. Liu, J. D. Howe, D. Tang and D. S. Sholl, *J. Phys. Chem. C*, 2018, **122**, 27486–27494.
28 E. D. Bloch, W. L. Queen, R. Krishna, J. M. Zadrozny, C. M. Brown and J. R. Long, *Science*, 2012, **335**, 1606–1610.
29 Z. Zhang, S. B. Peh, Y. Wang, C. Kang, W. Fan and D. Zhao, *Angew. Chem., Int. Ed.*, 2020, **132**, 19089–19094.
30 J. Pei, K. Shao, J. X. Wang, Y. Yang, Y. Cui, R. Krishna, B. Li and G. Qian, *Adv. Mater.*, 2020, **32**, 1908275.
31 L. Zhang, K. Jiang, L. Yang, L. Li, E. Hu, L. Yang, K. Shao, H. Xing, Y. Cui, Y. Yang, B. Li, B. Chen and G. Qian, *Angew. Chem., Int. Ed.*, 2021, **133**, 16131–16138.
32 H. Zeng, X. J. Xie, Y. Wang, D. Luo, R.-J. Wei, W. Lu and D. Li, *Chem. Sci.*, 2022, **13**, 12876–12882.
33 H. Zeng, M. Xie, Y. L. Huang, Y. Zhao, X. J. Xie, J.-P. Bai, M.-Y. Wang, R. Krishna, W. Lu and D. Li, *Angew. Chem., Int. Ed.*, 2019, **58**, 8515–8519.
34 L. Li, R. B. Lin, R. Krishna, H. Li, S. Xiang, H. Wu, J. Li, W. Zhou and B. Chen, *Science*, 2018, **362**, 443–446.
35 J. R. Li, R. J. Kuppler and H. C. Zhou, *Chem. Soc. Rev.*, 2009, **38**, 1477–1504.
36 R. T. Yang, *Adsorbents: Fundamentals and Applications*, Wiley, Hoboken, 2003.
37 M. Kang, S. Yoon, S. Ga, D. W. Kang, S. Han, J. H. Choe, H. Kim, D. W. Kim, Y. G. Chung and C. S. Hong, *Adv. Sci.*, 2021, **8**, 2004940.
38 O. T. Qazvini, R. Babarao, Z.-L. Shi, Y.-B. Zhang and S. G. Telfer, *J. Am. Chem. Soc.*, 2019, **141**, 5014–5020.

39 J. Pires, M. L. Pinto and V. K. Saini, *ACS Appl. Mater. Interfaces*, 2014, **6**, 12093–12099.
40 S. Jiang, L. Li, L. Guo, C. Song, Q. Yang, Z. Zhang, Y. Yang, Q. Ren and Z. Bao, *Sci. China: Chem.*, 2021, **64**, 666–672.
41 G. D. Wang, Y. Z. Li, W. J. Shi, H. Lei, Y.-Y. Wang and Z. Zhu, *Angew. Chem., Int. Ed.*, 2022, **134**, e202205427.
42 B. Zhu, J. Cao, S. Mukherjee, T. Pham, T. Zhang, T. Wang, X. Jiang, K. A. Forrest and M. J. Zaworotko, *J. Am. Chem. Soc.*, 2021, **143**, 1485–1492.
43 Z. Xu, X. Xiong, J. Xiong, R. Krishna, L. Li, Y. Fan, F. Luo and B. Chen, *Nat. Commun.*, 2020, **11**, 3163.
44 R. B. Lin, H. Wu, L. Li, X.-L. Tang, Z. Li, J. Gao, H. Cui, W. Zhou and B. Chen, *J. Am. Chem. Soc.*, 2018, **140**, 12940–12946.
45 Z. Di, C. Liu, J. Pang, S. Zou, Z. Ji, F. Hu, C. Chen, D. Yuan, M. Hong and M. Wu, *Angew. Chem., Int. Ed.*, 2022, **134**, e202210343.
46 S. B. Geng, E. Lin and X. Li, *J. Am. Chem. Soc.*, 2021, **143**, 8654–8660.
47 H.-G. Hao, Y.-F. Zhao, D.-M. Chen, J.-M. Yu, K. Tan, S. Ma, Y. Chabal, Z.-M. Zhang, J.-M. Dou, Z.-H. Xiao, G. Day, H.-C. Zhou and T.-B. Lu, *Angew. Chem., Int. Ed.*, 2018, **130**, 16299–16303.
48 G. D. Wang, R. Krishna, Y. Z. Li, W. J. Shi, L. Hou, Y. Y. Wang and Z. H. Zhu, *Angew. Chem., Int. Ed.*, 2022, **61**, e202213015.
49 X. W. Gu, J. X. Wang, E. Wu, H. Wu, W. Zhou, G. Qian, B. Chen and B. Li, *J. Am. Chem. Soc.*, 2022, **144**, 2614–2623.
50 J. W. Cao, S. Mukherjee, T. Pham, Y. Wang, T. Wang, T. Zhang, X. Jiang, H. J. Tang, K. A. Forrest, B. Space, M. J. Zaworotko and K.-J. Chen, *Nat. Commun.*, 2021, **12**, 6507.
51 P. Q. Liao, W. X. Zhang, J. P. Zhang and X.-M. Chen, *Nat. Commun.*, 2015, **6**, 8697.
52 H. Zeng, X.-J. Xie, M. Xie, Y. Huang, D. Luo, T. Wang, Y. Zhao, W. Lu and D. Li, *J. Am. Chem. Soc.*, 2019, **141**, 20390–20396.
53 X.-J. Xie, H. Zeng, M. Xie, W. Chen, G.-F. Hua, W. Lu and D. Li, *Chem. Eng. J.*, 2022, **427**, 132033.
54 H. Zeng, M. Xie, T. Wang, R.-J. Wei, X.-J. Xie, Y. Zhao, W. Lu and D. Li, *Nature*, 2021, **595**, 542–548.
55 T.-L. Hu, H. Wang, B. Li, R. Krishna, H. Wu, W. Zhou, Y. Zhao, Y. Han, X. Wang, W. Zhu, Z. Yao, S. Xiang and B. Chen, *Nat. Commun.*, 2015, **6**, 7328.
56 B. Li, X. Cui, D. O'Nolan, H.-M. Wen, M. Jiang, R. Krishna, H. Wu, R.-B. Lin, Y.-S. Chen, D. Yuan, H. Xing, W. Zhou, Q. Ren, G. Qian, M. J. Zaworotko and B. Chen, *Adv. Mater.*, 2017, **29**, 1704210.
57 R. B. Lin, L. Li, H. Wu, H. Arman, B. Li, R.-G. Lin and B. Chen, *J. Am. Chem. Soc.*, 2017, **139**, 8022–8028.
58 Y. Xie, Y. Shi, E. M. Cedeño Morales, A. E. Karch, B. Wang, H. Arman, K. Tan and B. Chen, *J. Am. Chem. Soc.*, 2023, **145**, 2386–2394.
59 R. B. Lin, L. Li, H. L. Zhou, H. Wu, C. He, S. Li, R. Krishna, J. Li, W. Zhou and B. Chen, *Nat. Mater.*, 2018, **17**, 1128–1133.
60 Z. Bao, J. Wang, Z. Zhang, H. Xing, Q. Yang, Y. Yang, H. Wu, R. Krishna, W. Zhou, B. Chen and Q. Ren, *Angew. Chem., Int. Ed.*, 2018, **130**, 16252–16257.
61 B. Liang, X. Zhang, Y. Xie, R.-B. Lin, R. Krishna, H. Cui, Z. Li, Y. Shi, H. Wu, W. Zhou and B. Chen, *J. Am. Chem. Soc.*, 2020, **142**, 17795–17801.
62 L. Yu, X. Han, H. Wang, S. Ullah, Q. Xia, W. Li, J. Li, I. da Silva, P. Manuel, S. Rudić, Y. Cheng, S. Yang, T. Thonhauser and J. Li, *J. Am. Chem. Soc.*, 2021, **143**, 19300–19305.
63 H. Wang, X. Dong, V. Colombo, Q. Wang, Y. Liu, W. Liu, X.-L. Wang, X.-Y. Huang, D. M. Proserpio, A. Sironi, Y. Han and J. Li, *Adv. Mater.*, 2018, **30**, 1805088.
64 A. Cadiau, K. Adil, P. M. Bhatt, Y. Belmabkhout and M. Eddaoudi, *Science*, 2016, **353**, 137–140.
65 H. Wang, X. Dong, V. Colombo, Q. Wang, Y. Liu, W. Liu, X.-L. Wang, X.-Y. Huang, D. M. Proserpio, A. Sironi, Y. Han and J. Li, *Adv. Mater.*, 2018, **30**, 1805088.
66 E. Velasco, S. Xian, L. Yu, H. Wang and J. Li, *Sep. Purif. Technol.*, 2022, **282**, 120010.
67 B. Liang, X. Zhang, Y. Xie, R.-B. Lin, R. Krishna, H. Cui, Z. Li, Y. Shi, H. Wu, W. Zhou and B. Chen, *J. Am. Chem. Soc.*, 2020, **142**, 17795–17801.
68 Y. Xie, Y. Shi, E. M. C. Morales, A. E. Karch, B. Wang, H. Arman, K. Tan and B. Chen, *J. Am. Chem. Soc.*, 2023, **145**, 2386–2394.
69 S. Tu, L. Yu, Y. Wu, Y. Chen, H. Wu, L. Wang, B. Liu, X. Zhou, J. Xiao and Q. Xia, *AIChE J.*, 2022, **68**, e17551.
70 L. Wang, W. Xue, H. Zhu, X. Guo, H. Huang and C. Zhong, *Angew. Chem., Int. Ed.*, 2023, **135**, e202218596.
71 L. Yu, S. Ullah, H. Wang, Q. Xia, T. Thonhauser and J. Li, *Angew. Chem., Int. Ed.*, 2022, **134**, e202211359.
72 X. Huang, S. Jiang, D. Ma, J. Xie, X. Feng and B. Wang, *Angew. Chem., Int. Ed.*, 2023, **62**, e202303671.
73 X.-P. Fu, Y.-L. Wang, X.-F. Zhang, Z. Zhang, C.-T. He and Q.-Y. Liu, *CCS Chem.*, 2022, **4**, 3416–3425.
74 M. Ding and H. L. Jiang, *CCS Chem.*, 2021, **3**, 2740–2748.
75 S. Yuan, L. Feng, K. Wang, J. Pang, M. Bosch, C. Lollar, Y. Sun, J. Qin, X. Yang, P. Zhang, Q. Wang, L. Zou, Y. Zhang, L. Zhang, Y. Fang, J. Li and H.-C. Zhou, *Adv. Mater.*, 2018, **30**, 1704303.